Fingerprint of climate change on Southern Ocean carbon storage

R. M. Wright[1], C. Le Quéré[1], N. Mayot[1], A. Olsen[2,3] and D. Bakker[1]

[1]School of Environmental Sciences, University of East Anglia, Norwich, NR4 7TJ, UK
[2]Geophysical Institute, University of Bergen, Bergen, Norway
[3]Bjerknes Centre for Climate Research, Bergen, Norway

Corresponding author: Rebecca M. Wright (rebecca.wright@uea.ac.uk)

Key Points:

- The effect of decadal climate variability on dissolved inorganic carbon in the Southern Ocean is nearly as large as that of atmospheric CO_2.
- Climatic drivers cause a distinct fingerprint on the concentration of dissolved inorganic carbon in the Southern Ocean interior.
- This fingerprint could serve to detect future trends in Southern Ocean carbon storage.

Abstract

The Southern Ocean plays a critical role in the uptake, transport and storage of carbon by the global oceans. It is the ocean's largest sink of CO_2, yet it is also among the regions with the lowest storage of anthropogenic carbon. This behaviour results from the unique combination of high winds driving the upwelling of deep waters and the subduction and northwards transport of surface carbon. Here we identify the indirect effect of climate-related changes in ocean conditions relative to the direct effect of anthropogenic changes in atmospheric CO_2 on the reorganisation of carbon in the Southern Ocean using a combination of modelling and observations. We show that the effect of climate variability and climate change on the storage of carbon in the Southern Ocean is nearly as large as the effect of anthropogenic CO_2 during the period 1998-2018 compared with a climatology around the year 1995. We identify a distinct climate fingerprint in dissolved inorganic carbon (DIC), with elevated DIC concentration in the surface ocean that reinforces the anthropogenic CO_2 signal, and reduced DIC concentration in the subsurface ocean that offsets the anthropogenic CO_2 signal. The fingerprint is strongest at lower latitudes (30°S-55°S). This fingerprint could serve to monitor the highly uncertain evolution of carbon within this critical ocean basin, and better identify its drivers.

1 Introduction

The Southern Ocean is one of the world's most important regions for the carbon cycle and the regulation of atmospheric CO_2 concentration, accounting for around a third of the global oceanic uptake of anthropogenic CO_2 resulting from human activities (Friedlingstein et al., 2021). Paradoxically, the Southern Ocean is also among the ocean basins with the lowest storage of anthropogenic carbon (Gruber et al., 2019a), especially considering its high uptake. This high uptake/storage ratio is caused by the unique combination of intense circumpolar winds driving the upwelling of deep waters that have not been in contact with the atmosphere for centuries, and the vigorous subduction and northwards transport of surface carbon within the Antarctic Intermediate Water and Subantarctic Mode Water.

Atmospheric conditions over the Southern Ocean have changed in recent decades, with winds strengthening in response to the depletion of stratospheric ozone reinforced by climate

change (Fyfe & Saenko, 2006; Thompson et al., 2011; Thompson & Solomon, 2002). Whereas the strengthening of the winds is clear over multiple decades, the effect on the vertical transport of water masses, and hence on the reorganisation of carbon within the ocean, is highly uncertain (Meredith et al., 2019). The difficulty comes from quantifying the relative effect of enhanced upwelling in response to the intensification of the winds, and the opposing effect of the intensification of eddies that results from the upwelling-driven steepening of isopycnals (Morrison et al., 2021). In addition, changes in sea-ice and buoyancy fluxes (precipitation and heat) are also altering vertical mixing and the transport of carbon, complicating the picture further. The latest assessment by the Intergovernmental Panel on Climate Change (IPCC) reports no consensus on the combined effects of these Earth System changes on the physical transport of water masses in the Southern Ocean due to conflicting evidence and poor model representations of key processes (Fox-Kemper et al., 2021). Uncertainties in physical changes translate directly into uncertainties in carbon changes, with carbon changes further compounded by potential changes in biological processes that are largely unknown. Wind variability also complexifies the detection of any longer-term trends.

Estimates based on carbon observations in the atmosphere and in the surface ocean have been used to infer changes and variability in recent decades, with evidence of periods of 'saturation' (Le Quéré et al., 2007) followed by 'reinvigoration' (Landschützer et al., 2015) of the Southern Ocean CO_2 sink. These decadal swings can only be explained by the large variability of the Southern Ocean in response to climatic change and/or variability, including that related to ozone depletion (Thompson et al., 2011). Estimates using ocean carbon models also show a response of the Southern Ocean CO_2 sink to climate variability, but models overwhelmingly produce a small climate response only that is almost entirely hidden by the large response to the rise in anthropogenic CO_2 (DeVries et al., 2019). Some of the model-data discrepancies could be explained by the paucity of observations, as differences are largest in locations with no observations (Hauck et al., 2020), and data gaps can lead to about 30% excessive variability in data products (Gloege et al., 2021). This limited evidence and quantitative understanding of the underlying processes means we currently have very little confidence in recent changes in the Southern Ocean carbon storage, and little insights into their likely persistence in the future.

Here we take advantage of the high ratio between the climatic and anthropogenic drivers of changes in carbon on decadal timescales within the Southern Ocean to identify the combined effect of climate-related changes relative to the direct anthropogenic changes on the reorganisation of carbon in the Southern Ocean, and the implications for the future. We identify a fingerprint for these two processes that could serve to monitor the evolution of carbon within this critical ocean basin.

We use a combination of modelling and observations to quantify the relative contribution of different drivers on the storage of DIC in the Southern Ocean. We use observations from the Global Ocean Data Analysis Project (GLODAP), a regularly updated synthesis of ocean surface and interior biogeochemical data (Olsen et al., 2020) and use PlankTOM12, a state-of-the-art Global Ocean Biogeochemical Model (GOBM) used in the Global Carbon Budget (GCB; Friedlingstein et al., 2021). We partition DIC into contemporary, anthropogenic and climate carbon (Fig. 1) and calculate the change in DIC inventory for each during the period 1998-2018 relative to a climatology centred around year 1995, providing a fingerprint in DIC. We use the model to directly attribute this climate fingerprint to various climatic drivers. Understanding how the Southern Ocean sink is responding to climate change and climate variability, is key to understanding how the global ocean sink will evolve over the coming decades.

2 Methods

2.1 The NEMO-PlankTOM12 Model Simulations

2.1.1 Model Description

PlankTOM12 is a global ocean biogeochemistry model with full marine cycles of key elements carbon, oxygen, phosphorus and silicon, and simplified cycles of nitrogen and iron. PlankTOM12 simulates plankton ecosystem processes and their interactions with the environment through the representation of 12 plankton functional types (PTFs). Spatial variability within PFTs is represented through parameter-dependence on environmental conditions including temperature, nutrients, light and food availability. PlankTOM12 represents sinking processes through the aggregation and disaggregation of organic material into two particles of different size classes, a small particle that sinks at a constant 3 m per day, and a large particle that sinks at a variable speed that depends on the ballasting of minerals (Buitenhuis et al.,

2013). For a full description of PlankTOM biogeochemistry see Wright et al. (2021) and Le Quéré et al. (2016).

PlankTOM12 is coupled online to the global ocean general circulation model Nucleus for European Modelling of the Ocean version 3.6 (NEMO v3.6-ORCA2). We used the global configuration with a horizontal resolution of 2° longitude by a resolution of 0.3° - 1.5° latitude using a tripolar orthogonal grid. The vertical resolution is 10 m for the top 100 m, decreasing to a resolution of 500 m at 5 km depth, with a total of 31 vertical z levels (Madec, 2013). The ocean is described as a fluid using the Navier–Stokes equations and a nonlinear equation of state (Madec, 2013). NEMO v3.6 explicitly calculates vertical mixing at all depths using a turbulent kinetic energy model and sub-grid eddy-induced mixing. The model is interactively coupled to a thermodynamic sea-ice model (LIM version 2; Timmermann et al., 2005).

2.1.2 Main Simulations

The PlankTOM12 simulations for this study are developed from the published simulations in the GCB 2021 (Friedlingstein et al., 2021), with the changes outlined below. Three simulations were devised in order to isolate the effects of climate change and climate variability from that of anthropogenic CO_2 (Table 1; sim^1, sim^2 and sim^3). sim^1 is designed as a control simulation that will be used to remove any residual model drift. It is forced by an atmospheric CO_2 of 278 ppm, including pre-industrial carbon in the initial conditions. The forcing fields are constant, which is achieved by looping over the daily fields for one year, therefore including no trends or variability in climate. sim^2 is designed to capture the effect of increasing anthropogenic CO_2 in the atmosphere. It is forced by the global observed monthly mean atmospheric CO_2, with the forcing fields looping over one year as in sim^1, therefore including trends and variability in anthropogenic CO_2 alone. sim^3 is the best estimate of the contemporary CO_2 fluxes. It is forced by the global observed monthly mean atmospheric CO_2 and by the daily forcing fields of the year of the simulation, therefore including trends and variability in both anthropogenic CO_2 and climate.

Each simulation is repeated three times, with a different forcing year for looping and spin-up. The forcing years are 1959, 1990 and 2013, selected as ‘representative’ years with no strong El Niño/La Niña present. Year 1990 is also the year used in the GCB GOBM ensemble

for looping and spin-up (Friedlingstein et al., 2021). sim^1 is run three times from 1750 to 2020, each repeating one of the three forcing years, keeping atmospheric CO_2 constant at 278ppm. sim^2 is run three times from 1750 to 2020, each repeating one of the three forcing years, with observed increasing atmospheric CO_2. sim^3 is initialised three times, from each of the three sim^2 simulations in 1947, and then each is run until 2020 with daily observed forcing fields and observed increasing atmospheric CO_2.

For sim^1, sim^2 and sim^3, the three members (forcing years 1959, 1990, and 2013) are averaged. These 3-member averages are then combined in a variety of ways to isolate drivers of trends in ocean DIC;

$$DIC_{CO}^{mod} = sim^3 - sim^1 \quad (1)$$

$$DIC_{AN}^{mod} = sim^2 - sim^1 \quad (2)$$

$$DIC_{CL}^{mod} = DIC_{CO}^{mod} - DIC_{AN}^{mod} \quad (3)$$

Where contemporary DIC (DIC_{CO}^{mod}) includes climate variability, climate change and increasing anthropogenic CO_2 with the model drift removed. Anthropogenic DIC (DIC_{AN}^{mod}) includes increasing anthropogenic CO_2, without climate variability or climate change, with the model drift removed. Climate DIC (DIC_{CL}^{mod}) includes climate variability and climate change, without anthropogenic CO_2, with the model drift removed.

The PlankTOM12 three-member ensemble mean is within the GCB multi-model range for its representation of the contemporary and anthropogenic CO_2 signals (Fig. 1a, b), but it has a stronger climate signal compared to the other models for the period 1960-1985 (Fig. 1c). This stronger signal is due to the specifics of the spin up combined with the use of NCEP forcing, which is known for its strong trend in Southern Ocean winds. GCB models use a mixture of NCEP, JRA and ERA forcing fields (Friedlingstein et al., 2021). After 1985, and throughout the period focused on in this study, the climate ensemble is within the GCB multi-model standard deviation (Fig. 1c).

2.1.3 Forcing Simulations

Two additional PlankTOM12 simulations were carried out to isolate the influence of wind stress on ocean circulation and the influence of wind speed on air-sea gas exchange from the overall climate influence (Table 1; sim^4 and sim^5).

$$DIC_{WSP}^{mod} = sim^3 - sim^4 \quad (4)$$

$$DIC_{WST}^{mod} = sim^3 - sim^5 \quad (5)$$

The remaining effect of buoyancy forcing was then calculated using these two simulations.

$$DIC_{BUO}^{mod} = DIC_{CL}^{mod} - (DIC_{WSP}^{mod} + DIC_{WST}^{mod}) \quad (6)$$

Buoyancy, therefore, accounts for the remaining climate forcing not included in wind speed or wind stress, including air temperature, humidity, cloud cover, precipitation and surface pressure.

Table 1. PlankTOM12 model simulations and the formulations used to isolate drivers of changes in carbon. Each sim[1-5] was run with each of the three spin-up years, 1959, 1990 and 2013, and the 3-member ensemble average is presented in the text. Variable wind stress influences ocean circulation, while variable wind speed influences the CO_2 gas exchange.

	Drift	**pre-Industrial carbon**	**Atmospheric CO_2**	**Variable Climate**	**Variable Wind Speed**	**Variable Wind Stress**	**Variable Buoyancy**
Simulation							
sim^1	Y	Y					
sim^2	Y	Y	Y				
sim^3	Y	Y	Y	Y	Y	Y	Y
sim^4	Y	Y	Y	Y		Y	
sim^5	Y	Y	Y	Y	Y		
Formulation							
Contemporary (Eq. 1)			Y	Y	Y	Y	Y
Anthropogenic (Eq. 2)			Y				
Climate (Eq. 3)				Y	Y	Y	Y

Wind Speed (Eq. 4)					Y		
Wind Stress (Eq. 5)						Y	
Buoyancy (Eq. 6)							Y

174

Figure 1: Southern Ocean CO_2 flux in GOBMs for contemporary (a), anthropogenic (b) and climate (c) carbon (PgC/yr). The monthly PlankTOM12 three-member ensemble mean used in this study is shown by the coloured lines with the ensemble min/max (coloured shading). The yearly Global Carbon Budget multi-model mean is shown by the thick grey lines with the ± 1 standard deviation (grey shading). Each individual GCB model is shown by the thin grey lines. Carbon is partitioned into contemporary (from increasing atmospheric CO_2, climate change, and climate variability), anthropogenic (from increasing atmospheric CO_2 only), and climate (from climate change and climate variability, calculated as the difference between contemporary and anthropogenic carbon).

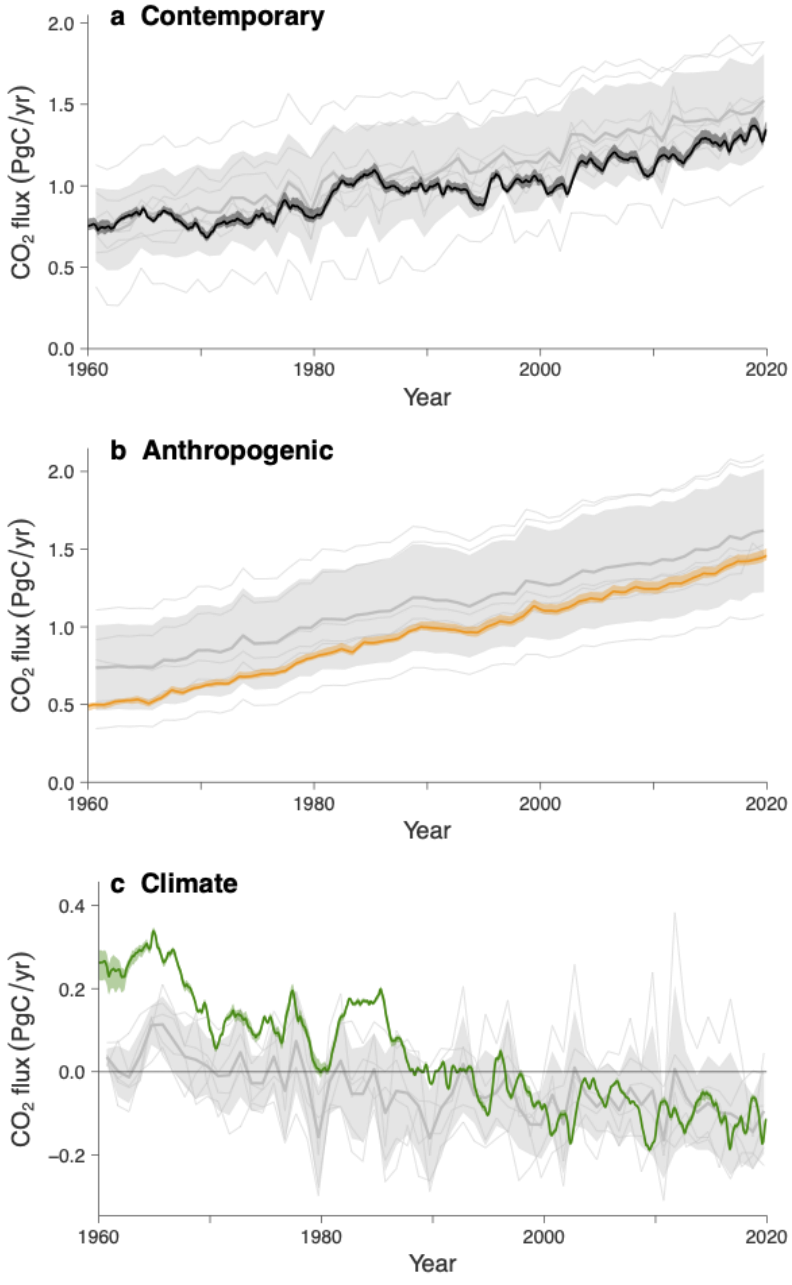

2.2 Observational Data

The contribution of growing atmospheric CO_2 and climate change and variability can be isolated thanks to the growing number and quality of ocean observations. The GLODAP database (Olsen et al., 2020) provides DIC observations for the Southern Ocean, quality controlled, back to the 1970s. For the first two decades, data was sparse in both space and time and substantial biases in these data have been identified. During the 1990's coverage and consistency of data greatly increased, and these improvements continued over subsequent decades (Olsen et al., 2020). DIC changes in inventory for the contemporary, anthropogenic, and climate effects on carbon are calculated using GLODAP observations of DIC and nitrate (GLODAPv2.2020; Olsen et al., 2020), and climatologies of DIC (Broullón et al., 2020) and nitrate (Broullón et al., 2019), derived from GLODAP using a neural network approach, centred on 1995.

The GLODAP merged master files for DIC and nitrate were gridded onto the PlankTOM12 model grid, with 31 vertical z levels and into monthly means. The two climatologies were gridded onto the PlankTOM12 model grid. The climatologies were then subsampled to GLODAP. The GLODAP database undergoes extensive and systematic quality control and bias checks (Olsen et al., 2020) and so no further exclusion of data was carried out.

2.3 Observational Change in DIC Inventory

The change in DIC inventory for the period 1998 to 2018 are calculated for the three carbon types (Contemporary, Anthropogenic and Climate) for both observations and the model. The observed Contemporary change in DIC inventory (ΔDIC_{CO}^{obs}) is calculated as follows:

$$\Delta DIC_{CO}^{obs} = DIC_{CO}^{obs} - DIC_{clim}^{obs} \quad (7)$$

Where DIC_{CO}^{obs} is GLODAPv2.2020 gridded DIC observations averaging all data points as a function of latitude from January 1998 to April 2018, and DIC_{clim}^{obs} is climatological of DIC centred on 1995 (Broullón et al., 2020). This 1998-2018 time period was selected because 1) it begins after the assumed 5-year climatology of 1995, 2) it includes the most recent observations available in the Southern Ocean for this GLODAP update, 3) it begins in the period when data coverage greatly increased and required data adjustments decreased (Olsen et al., 2020), and 4) it

covers a long enough period to remove interannual and reduce interdecadal variability to uncover long-term trends.

Observed Anthropogenic (ΔDIC_{AN}^{obs}) and Climate (ΔDIC_{CL}^{obs}) carbon changes in inventory are estimated following the method in Bronselaer et al. (2020);

$$\Delta DIC_{AN}^{obs} = \Delta DIC_{CO}^{obs} - \Delta DIC_{CL}^{obs} \quad (8)$$

$$\Delta DIC_{CL}^{obs} = \frac{117}{16} \times \Delta NO_{CO}^{obs} \quad (9)$$

Where 117/16 is the Redfield Ratio between carbon and nitrogen, multiplied by the Contemporary nitrogen change in inventory (ΔNO_{CO}^{obs});

$$\Delta NO_{CO}^{obs} = NO_{CO}^{obs} - NO_{clim}^{obs} \quad (10)$$

Where NO_{CO}^{obs} is GLODAPv2.2020 nitrate observations, co-located with the DIC observations, from January 1998 to April 2018, and NO_{clim}^{obs} is a climatology of nitrate centred on 1995 (Broullón et al., 2019). Nitrate can be used to derive climate influences on DIC as its concentration is dominated by dynamic changes, and less influenced by temperature than oxygen is (Bronselaer et al., 2020).

We quantify the GLODAPv2.2020 dataset observational uncertainty, adapting the method from Bronselaer et al. (2020). Dataset uncertainty is separated into the random error and the observed variability.

$$\sigma^2 = \sqrt{\frac{\sigma_{random}^2}{n} + \sigma_{variability}^2} \quad (11)$$

The random error (*random*) given for the dataset after error correction is described as being consistent to better than 4 μmol/kg (Olsen et al., 2020). This is divided by the number of data points used for the shown mean (*n*). This dataset error is added in quadrature to the uncertainty due to natural variability (*variability*), taken as the standard deviation of the shown mean, along the time, latitude and longitude axes.

2.4 Model Change in DIC Inventory

The modelled change in DIC inventory (ΔDIC^{mod}) is calculated;

$$\Delta DIC_{C}^{mod} = DIC_{C}^{mod} - DIC_{climC}^{mod} \quad (12)$$

Where C is substituted for each carbon type (CO, AN, CL from Eq. 4-6), DIC^{mod} is the PlankTOM12 simulation for the relevant carbon type from January 1998 to April 2018 and DIC_{clim}^{mod} is a climatology of the PlankTOM12 simulation for the relevant carbon type using January 1993 to December 1997.

The PlankTOM12 change in DIC inventory is given both as the full model output, and as the model output subsampled to GLODAPv2.2020 observational coverage spatially and temporally. The similarity between the full and subsampled model ensemble fingerprints provides evidence that the observations are not substantially biassed by patchy data collection (Fig. 2). A unit conversion is carried out on the model output from μmol/L to μmol/kg, to match the observational units. The conversion is carried out using in-situ density, temperature and salinity from the model output.

3 Results

3.1 Detection of a Southern Ocean climate fingerprint

In the surface ocean, observations show that both anthropogenic CO_2 and climatic drivers act to increase DIC concentration, with the strength of the signal for both increasing at higher latitudes (North of 55°S; Fig. 2). In the subsurface ocean, climatic drivers act to decrease DIC concentration, opposing the influence of increasing anthropogenic CO_2, with a stronger decrease at higher latitudes (North of 55°S). These patterns result in a climate fingerprint specific to Southern Ocean change and were detectable in both the observations and the model (Fig. 2). The fingerprint of climate dynamics is apparent in the negative subsurface DIC, which indicates ventilation of natural carbon via transport out of deep water in the upper cell, where it is either upwelled into the mixed layer and outgassed or subducted into the mode and intermediate water to the north, where it reinforces the anthropogenic carbon signal (Fig. 2).

In the recent past the signature of climate variability and climate change is as large as that of anthropogenic CO_2 (Fig. 3). Over the period analysed here, the observations suggest that the natural carbon in the Southern Ocean has changed in a way that limits the absorption of further atmospheric carbon due to a change in the sea-air gradient in pCO_2. For the contemporary signal, the model and observations show a similar magnitude of change both at the surface and at depth.

For the anthropogenic signal, the model is similar to the observations at the surface, while underestimating the signal at depth. For the climate signal, the model underestimates the observations at the surface, while showing a similar magnitude of change at depth (Fig. 3). The observed climate signal at depth is distinct from the anthropogenic signal but it is not distinct from zero (Fig. 3).

The modelled climate fingerprint of increasing DIC at the surface and decreasing DIC at the subsurface at higher latitudes (North of 55°S) is detectable across the three ocean basins, with spatial variability in the signal strength (Fig. 4). The modelled climate change in inventory signal shows hotspots in the Pacific basin and south-east Indian basin, consistent with upwelling in regions of intense mode and intermediate water formation (Downes et al., 2017) (Fig. 4). Zonal variations in upwelling strength, mixed-layer depth, and mode and intermediate water formation drive the zonal variation in the change in inventory (Downes et al., 2017; Gruber et al., 2019b; Morrison et al., 2021; Sallée et al., 2010).

The model underestimates the positive influence of climatic drivers at the surface at lower latitudes (<55°S), leading to a general underestimation of contemporary surface carbon increase compared to observations (Fig. 3). Despite this underestimation, the model also produces a pattern associated with the upper limb of the overturning circulation and the northward transport of anthropogenic CO_2 and its storage into mode and intermediate water masses (Gruber et al., 2019b), with the relatively shallow anthropogenic carbon penetration at higher latitudes and deeper penetration at lower latitudes (<55°S; Fig. 2). The model analysis shows that the fingerprint in the observations is unlikely to be due to sampling bias, as subsampling the model to the observations does not change the fingerprint pattern (Fig. 2). The fingerprint is also unlikely to be due to the summer sampling bias in Southern Ocean observations (Olsen et al., 2020), as the fingerprint persisted when the observed changes in inventory were separated into seasons (not shown here).

Figure 2: Zonally-averaged change in DIC inventory in the Southern Ocean, for 1998-2018 minus 1995 (µmol/kg). The change in inventory for the contemporary DIC (a, b, c) is partitioned into the direct contribution of anthropogenic CO_2 (d, e, f) and the contribution of climate variability and climate change (g, h, i). Estimates are based on the PlankTOM12 model ensemble (a, d, g), on the PlankTOM12 model ensemble subsampled to the GLODAP observations (b, e, h), and on the GLODAP observational data (c, f, i).

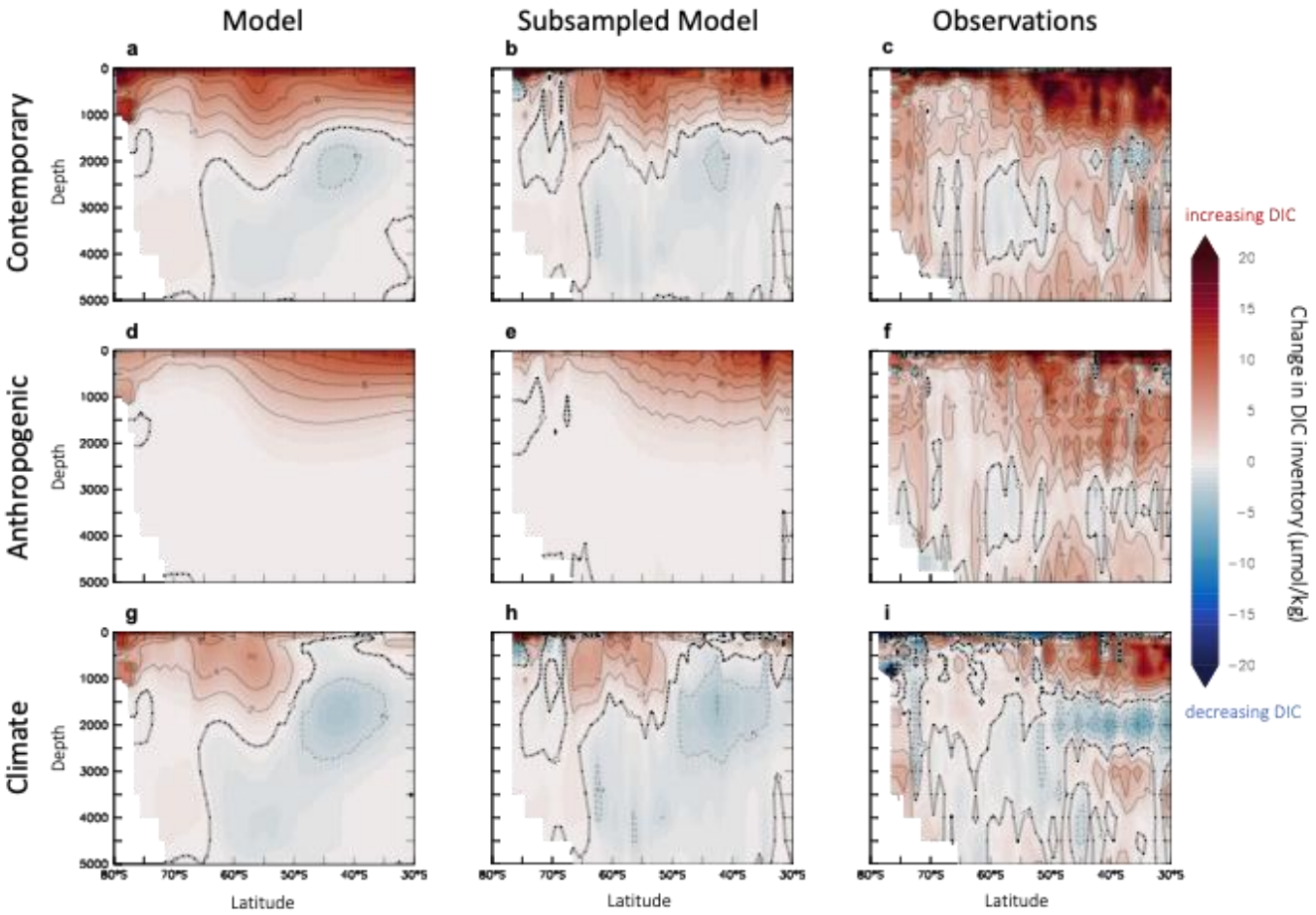

Figure 3: Zonally-averaged change in DIC inventory in the Southern Ocean, for 1998-2018 minus 1995 (µmol/kg). The change in inventory is separated into two depth slices averaged over 300-600m (a-b) and at 2000m (c-d). The change in inventory for the contemporary DIC (a, c) is partitioned into the direct contribution of anthropogenic CO_2 and the contribution of climate variability and climate change (b, d). Solid lines show the mean and shading shows the error (see method for details) for observations, dashed lines show the mean for the subsampled PlankTOM12 model ensemble. The depth slice of 300-600m is used as it is below strong seasonal influence, helping to reduce noise from seasonal variability. The depth slice of 2000m is used as the depth level with the strongest observed climate signal. The gridded data represent a depth thickness of 375m for both these depths.

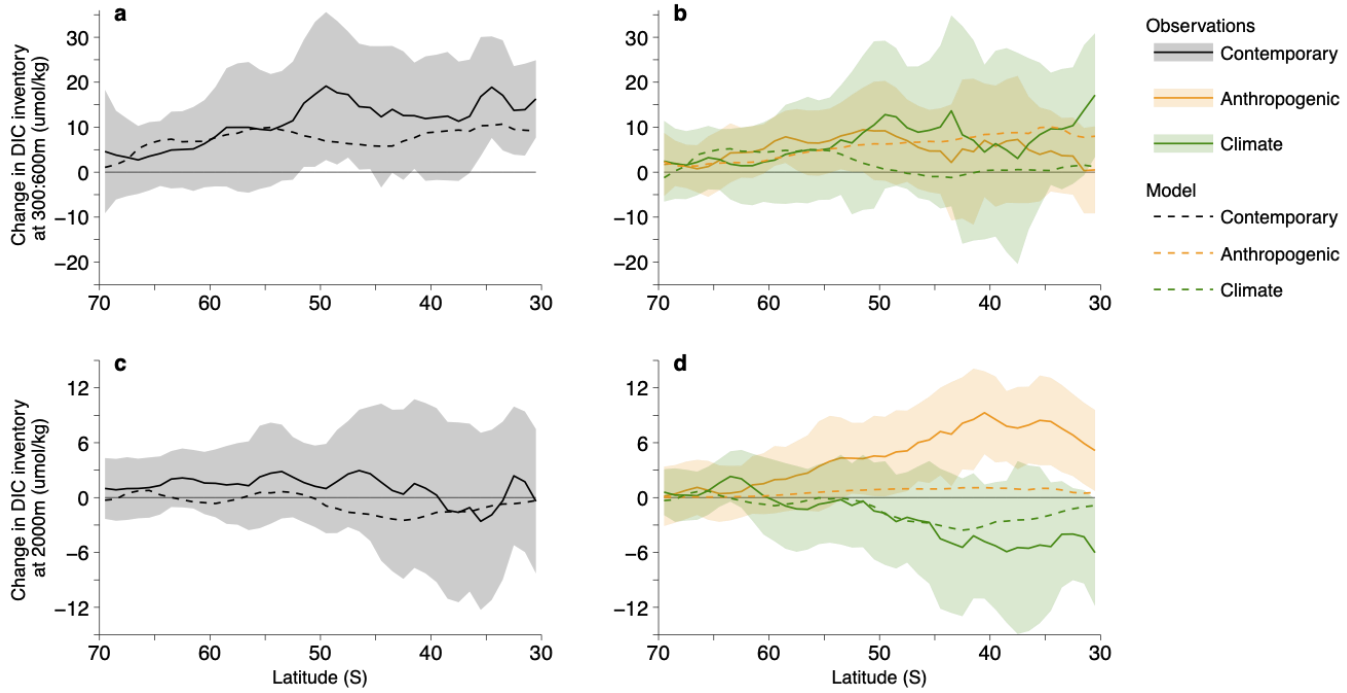

Figure 4: Modelled change in DIC inventory in the Southern Ocean, for 1998-2018 minus 1995 (μmol/kg). The PlankTOM12 ensemble change in inventory is separated into two depth slices averaged over 300-600m (a-c) and 2000m (d-f). The change in inventory for the contemporary DIC (a, d) is partitioned into the direct contribution of anthropogenic CO_2 (b, e) and the contribution of climate variability and climate change (c, f). The depth slice of 300-600m is used as it is below strong seasonal influence, helping to reduce noise from seasonal variability. The depth slice of 2000m is used as the depth level with the strongest observed climate signal. The gridded data represent a depth thickness of 375m for both these depths. Longitude lines show the boundaries of ocean basins.

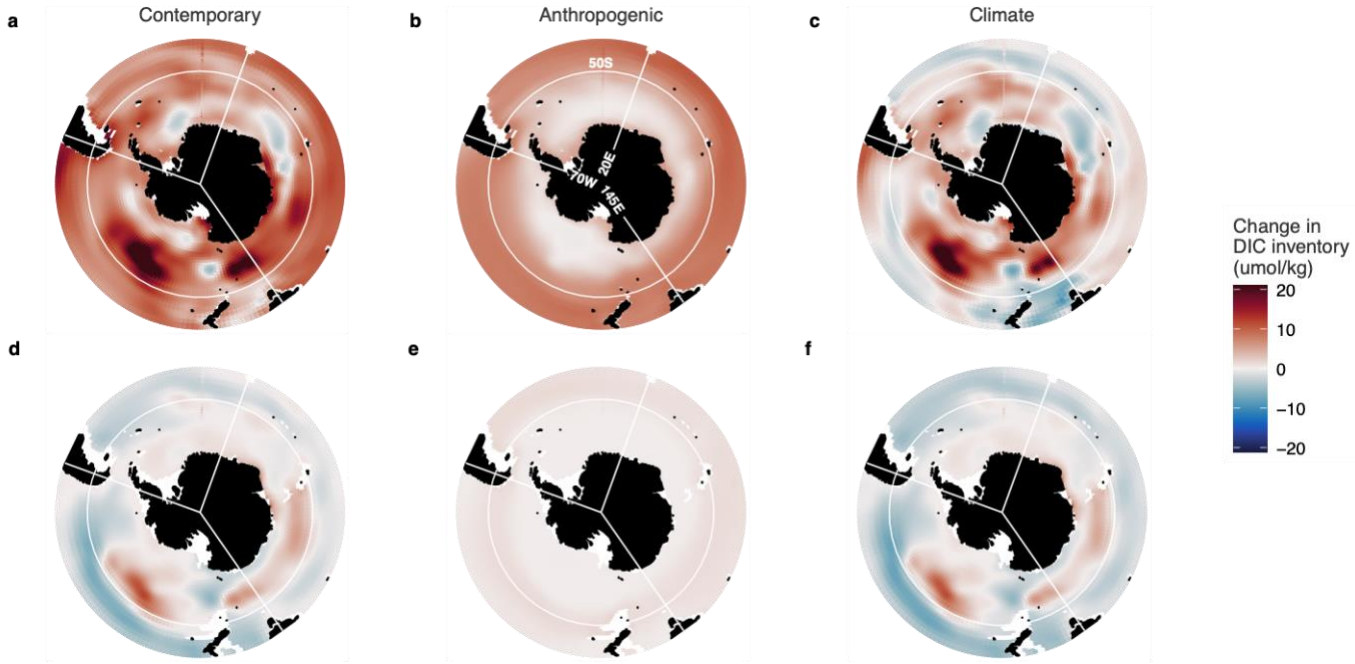

3.2 Contribution of natural climate drivers to the climate fingerprint

Overturning in the Upper Cell transports old water containing natural carbon, from the subsurface to the surface via upwelling, where it is outgassed or transported northward and subducted, mixing with anthropogenic carbon uptake from the atmosphere and forming mode and intermediate waters as it crosses the base of the mixed layer. The maximum mixed layer depth (MLD) occurs in winter due to enhanced wind-driven mixing and buoyancy loss (Patara et al., 2021; Sallée et al., 2010). Seasonal re-stratification in spring shallows the MLD, isolating waters at the bottom of the winter mixed layer from the atmosphere, forming mode and intermediate waters. Biological export production has also been shown to play a role in the transport of carbon through repackaging processes (Gruber et al., 2019b; MacGilchrist et al., 2019).

Without the contribution of the climate signal on DIC, the surface change in inventory in contemporary DIC would be reduced by a factor of almost two north of 55°S, and the subsurface change in inventory in contemporary DIC would be increased by a factor of almost two (Fig. 3). The effect of climate change and variability on DIC, therefore, has a substantial contribution to the gradient between the surface and subsurface contemporary carbon, limiting the absorption of further atmospheric carbon due to a change in the sea-air gradient in pCO_2. Within the model, we use this DIC fingerprint to assess the contribution of natural drivers to the climate fingerprint.

We conduct additional model simulations to separate the climate signal into the contribution of wind speed on air-sea CO_2 gas exchange, the effect of wind stress on ocean circulation and the effect of effects of buoyancy fluxes (driven by air temperature, humidity, cloud cover, precipitation and surface pressure; see section 2.1.3 and Table 1). Wind stress acts to increase the DIC inventory south of 50°S and decrease the DIC inventory north of 50°S, both at the surface and at depth (Fig. 5). The strongest increase occurs between 55-65°S in the surface while the strongest decrease occurs between 40-45°S at depth. The effects of wind stress on ocean circulation include the vertical and horizontal transport of water through changes in upwelling as well as surface dynamical changes through wind-driven mixing.

The effect of wind speed and buoyancy are small compared to that from wind stress (Fig. 5). In the surface, south of 50°S, wind speed and buoyancy act in opposition and mostly cancel each other out, while north of 50°S they both increase the DIC inventory by around 1 μmol/kg (Fig. 5a). At depth, south of 50°S, the wind speed effect is close to zero and the buoyancy effect is small, between 0 and -1 μmol/kg. At depth, north of 50°S, wind speed and buoyancy act in opposition and mostly cancel each other out (Fig. 5b). The climate DIC fingerprint is dominated by the effect of wind stress on ocean circulation (Fig. 5), especially in the regions where wind speed and buoyancy act in opposition, in the surface south of 50°S (Fig. 5a) and at depth, north of 50°S (Fig. 5b).

Figure 5: Zonally-averaged modelled change in DIC inventory in the Southern Ocean, for 1998-2018 minus 1995 (µmol/kg). The PlankTOM12 ensemble change in inventory is separated into two depth slices averaged over 300-600m (a) and 2000m (b). The change in inventory for climate DIC is partitioned into the direct contribution of wind speed (on air-sea CO_2 gas exchange), wind stress (on ocean circulation) and buoyancy fluxes (driven by air temperature, humidity, cloud cover, precipitation and surface pressure). The depth slice of 300-600m is used as it is below strong seasonal influence, helping to reduce noise from seasonal variability. The depth slice of 2000m is used as the depth level with the strongest observed climate signal. The gridded data represent a depth thickness of 375m for both these depths.

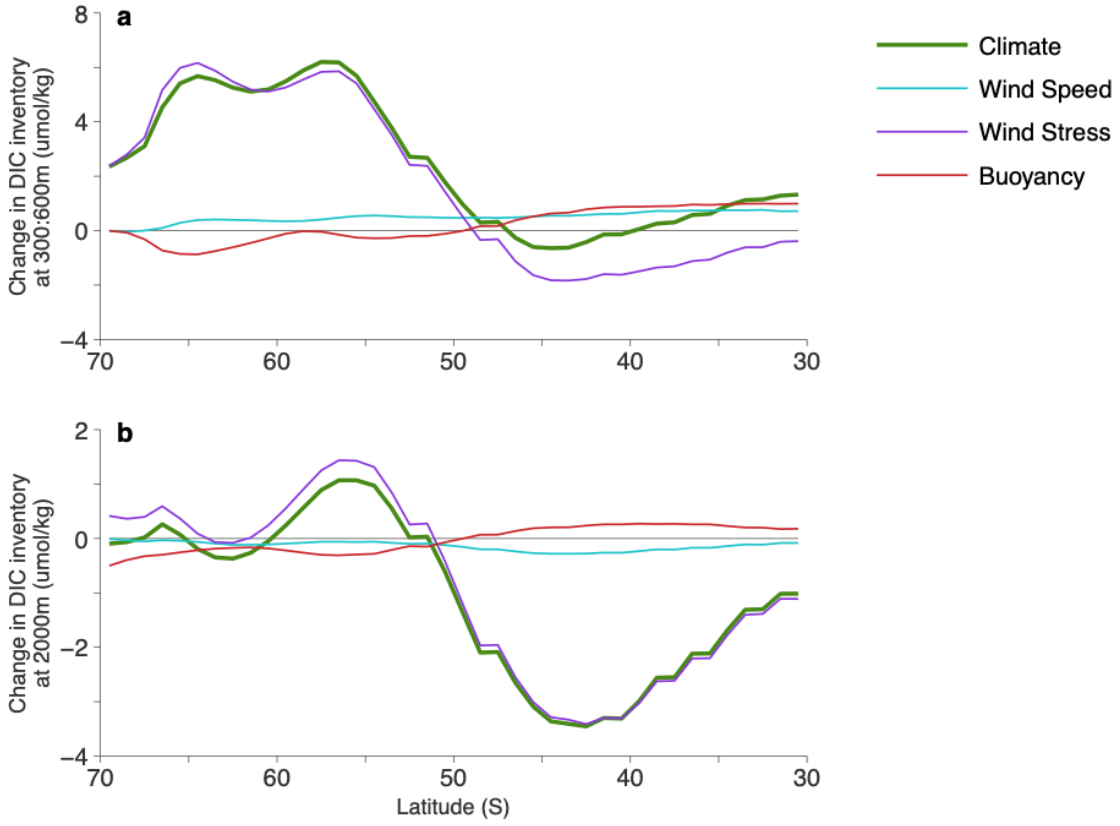

3.3 Climate fingerprint over time & implications for the Southern Ocean Carbon Flux

Interdecadal variability in DIC trends is expected, following patterns of saturation and reinvigoration found in studies of surface carbon fluxes (Keppler & Landschützer, 2019; Landschützer et al., 2015; Le Quéré et al., 2007). In Figure 6, the observed climate DIC change in inventory is decomposed into 5-year time periods. At 2000m, there is minimal change for 1998:2002, followed by a sharp decrease for 2003:2007 down to a mean of -7.3 µmol/kg, with the uncertainty not quite distinct from zero. After this minimum the inventory at 2000m

gradually increases over time to -5.9 and -4.6 μmol/kg (Fig. 6a). At 300:600m, the maximum change in inventory is for 1998:2002 with a mean of 12.2 μmol/kg, after this, the inventory decreases to between 4.8 and 7.7 μmol/kg without a clear trend over time (Fig 6a). Over the full period (1998:2018) the observed climate DIC change in inventory is 7.0 μmol/kg at 300:600m and -5.2 μmol/kg at 2000m (Fig. 6b).

The upwelling of natural carbon limits the amount of atmospheric CO_2 that the ocean can absorb. This mechanism in the Southern Ocean is already well documented and understood (Lenton et al., 2013; Gruber et al., 2019b), our work (Fig. 6) indicates that this mechanism may have increased over recent decades, with implications for the future strength of the SO carbon flux, if this fingerprint persists. Following the logic of enhanced upwelling bringing more climate carbon from depth to surface waters, the saturation period (pre-2002) (Landschützer et al., 2015; Le Quéré et al., 2007) can be assumed to coincide with an increase in climate DIC at the surface (and smaller negative change in inventory at depth), so higher climate carbon in surface waters reduces the sea-air difference in carbon, reducing the uptake of atmospheric CO_2. An increase in the climate change in inventory at the surface and small change in inventory at depth is shown in the observations here for the period 1998:2002 (Fig. 6). The reinvigoration period (2003-2012) (Landschützer et al., 2015) can then be assumed to coincide with a decrease in climate DIC inventory at the surface (and larger negative change in inventory at depth), so lower climate carbon in surface waters increases the sea-air difference in carbon, increasing the uptake of atmospheric CO_2. This decrease in climate DIC change in inventory at the surface and larger negative change in inventory at depth for the period 2003:2012 can also be detected here in the observations (Fig. 6).

Figure 6: Zonally-averaged observed change in climate DIC inventory in the Southern Ocean, for 1998-2018 minus 1995 (µmol/kg). The change in inventory is averaged over 43°S-33°S and separated into two depth slices averaged over 300-600m (a-c) and 2000m (d-f). The change in inventory is shown as 5-year time intervals (a) and over the full period (b). Circles show the mean and error bars show the error (instrumental error and natural variability over time, longitude, latitude and depth, see method for details). The depth slice of 300-600m is used as it is below strong seasonal influence, helping to reduce noise from seasonal variability. The depth slice of 2000m is used as the depth level with the strongest observed climate signal. The gridded data represent a depth thickness of 375m for both these depths.

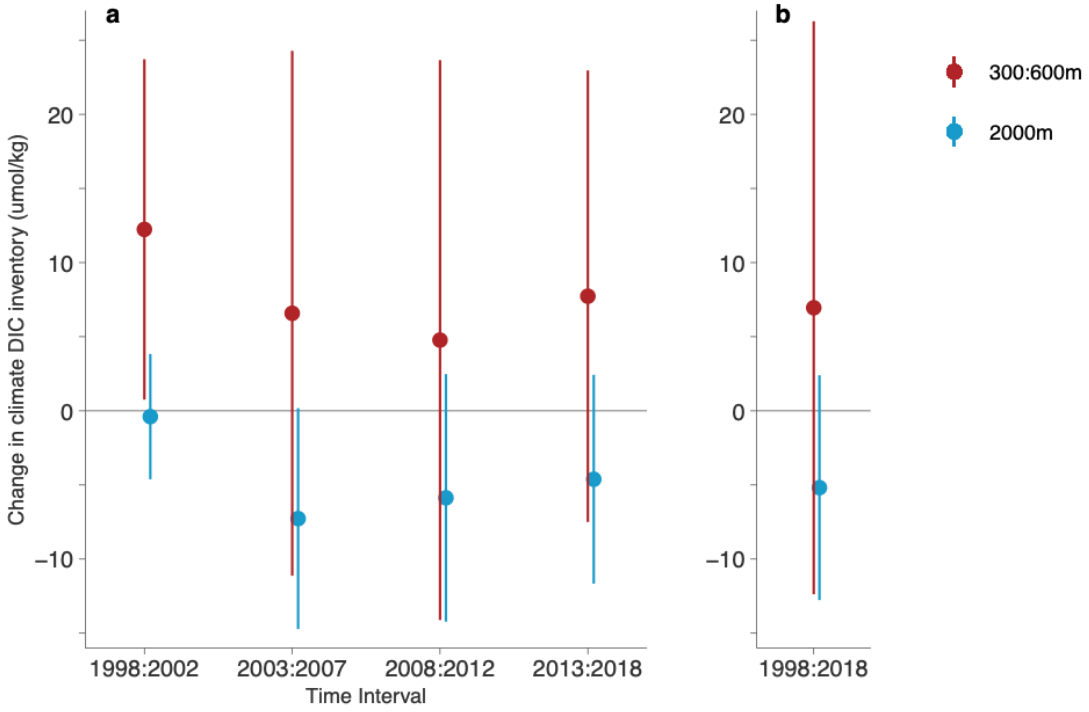

4 Discussion & Conclusion

Using a combined analysis of observations and a model, we showed that the impact of climate change and variability on DIC is as large as the impact of changing atmospheric CO_2 concentration in the Southern Ocean over the period 1998 - 2018. This signal is specific to the Southern Ocean because of the unique combination of highly variable winds, strong upwelling, and subduction and northward transport of surface DIC. This unique property means that the Southern Ocean is an ideal location to detect the fingerprint of climate change on DIC.

Our model analysis suggests that strong winds lead to a specific fingerprint with enhanced DIC in the surface and decreased DIC in the sub-surface, which is driven by changes in upwelling. Such a fingerprint is also detected in the observations with the surface and sub-

surface DIC signals distinct from each other. However, the sub-surface signal is not distinct from zero in the observed estimate, and the modelled climate signal is larger than other similar models. Therefore a firm attribution cannot yet be done. If the signal is indeed caused by increasing winds, and the winds continue to increase from the combination of slow ozone recovery and continued global warming, the fingerprint should emerge distinctly from zero in the future. The collection of in-situ nitrate data in addition to DIC at a depth of around 2000m between 50°S and 30°S is identified here as key to track climate-driven changes in carbon in the Southern Ocean.

Our results concur with a recent review on carbon in the Southern Ocean that highlights that while there are several published estimates of changes in anthropogenic carbon, there is no equivalent for changes in climate carbon (Gruber et al., 2019b). Our analysis of the GLODAP observations concurs with the periods of 'saturation' (Le Quéré et al., 2007) and 'reinvigoration' (Landschützer et al., 2015) of the Southern Ocean carbon sink, adding to the evidence of the mechanisms driving these shifting trends. DeVries et al. (2017) show how changes in the upper ocean (0-1000m) overturning circulation for the 1980's to the 2000's may have affected climate and anthropogenic carbon fluxes, with weakening overturning in the 2000s reducing outgassing of natural CO_2 and increasing the uptake of anthropogenic CO_2, thus increasing the total carbon flux. Our findings agree with this mechanism and highlight that stronger overturning (associated with stronger winds) decreases the carbon flux from the atmosphere to the ocean. McKinley et al. (2020) attributes the variability of the global sink to external forcing, namely the variable growth rate of atmospheric CO_2, where the slowed growth rate of atmospheric CO_2 results in a slowed ocean carbon sink. While our findings suggest that the effect of climate variability and climate change on CO_2 fluxes is nearly as large as that of rising atmospheric CO_2 in the Southern Ocean over the last decades, with most of the variability coming from climate effects.

Our findings differ from those in Bronselaer et al., (2020). In their study, the climate (dynamic) DIC change in inventory increases more in the surface south of 60°S, while here we find the change in inventory increases more in the surface north of 60°S compared to south. Our subsurface findings cannot be compared as they only looked above 2000m, and only find significance much shallower from around 500m. They find that wind-driven mixing and meltwater effects (within buoyancy here) reinforce each other in the surface south of 60°S (Bronselaer et al., 2020), while we find that for the same region buoyancy counteracts wind-

460 driven mixing. The key reasons behind these differences include; the change in inventory being
461 calculated with a time period of 2014:2019 minus 1985:2005; different observational datasets
462 (SOCCOM for later period and GLODAP ship-board for earlier period), and in our study
463 buoyancy is driven by air temperature, humidity, cloud cover, precipitation and surface pressure,
464 while they look at meltwater effects specifically (Bronselaer et al., 2020). These differences in
465 model setup, observations and time periods likely account for much of the difference between
466 findings.

467 Model improvements could include a higher resolution allowing for meso-scale eddy
468 parameterisation to compare against the current eddy resolving model, testing different ice
469 models to see if there is a change in the wind/buoyancy relationship around the Antarctic
470 coastline, and testing different wind forcing products to see if they affect both the strength and
471 the timing of the climate fingerprint. The next steps for this work could also include updating the
472 change in inventory with new GLODAP releases to extend the time period, and testing other
473 methods of separating contemporary carbon into anthropogenic and climate i.e. the eMLR(C*)
474 method, which uses observed alkalinity and phosphate along with an extended multiple linear
475 regression (Clement & Gruber, 2018). Both the eMLR(C*) method and the method used in this
476 study utilise biogeochemical observations other than DIC to separate contemporary carbon, each
477 with different benefits and drawbacks.

478 We identify a distinct climate fingerprint in observed Southern Ocean DIC. Our model
479 analysis suggests that this contemporary DIC fingerprint can be explained by a combination of
480 anthropogenic carbon ventilation of surface waters, and climate carbon redistribution from
481 subsurface to surface waters, reducing climate carbon in the subsurface while enhancing it in the
482 surface. Observations over a longer time period, and models with more complete processes, will
483 be needed before confirming the presence of a trend. We show here that measurements that keep
484 track of this distinct fingerprint may facilitate the early detection of climate-driven trends in DIC
485 reorganisation in the Southern Ocean interior.

486

Acknowledgments

R.M.W. and N.M. were funded by UK's Natural Environment Research Council (SONATA: grant no. NE/P021417/1). N.M. also received funding from the European Commission EC H2020 (4C; grant no. 821003). C.L.Q. was funded by the UK Royal Society (grant no. RP\R1\191063). AO appreciates funding from EU H2020 project COMFORT (grant no. 820989).

Thanks to Erik Buitenhuis and David Willis for their work on the NEMO-PlankTOM12 model development.

Thanks to the many scientists involved in all stages of producing the invaluable GLODAP database.

The research presented in this paper was carried out on the High Performance Computing Cluster supported by the Research and Specialist Computing Support service at the University of East Anglia.

There are no conflicts of interest that the authors are aware of.

Open Research

The data that support the findings of this study are published openly at: GLODAP (https://www.glodap.info/). The NEMO-PlankTOM12 simulations used in this study are available on request from the lead author.

References

Bronselaer, B., Russell, J. L., Winton, M., Williams, N. L., Key, R. M., Dunne, J. P., et al. (2020). Importance of wind and meltwater for observed chemical and physical changes in the Southern Ocean. *Nature Geoscience*, *13*(1), 35–42. https://doi.org/10.1038/s41561-019-0502-8

512 Broullón, D., Pérez, F. F., Velo, A., Hoppema, M., Olsen, A., Takahashi, T., et al. (2019). A
513 global monthly climatology of total alkalinity: a neural network approach. *Earth System*
514 *Science Data*, *11*(3), 1109–1127. https://doi.org/10.5194/essd-11-1109-2019
515 Broullón, D., Pérez, F. F., Velo, A., Hoppema, M., Olsen, A., Takahashi, T., et al. (2020). A
516 global monthly climatology of oceanic total dissolved inorganic carbon: A neural
517 network approach. *Earth System Science Data*, *12*(3), 1725–1743.
518 https://doi.org/10.5194/essd-12-1725-2020
519 Buitenhuis, E. T., Hashioka, T., & Le Quéré, C. (2013). Combined constraints on global ocean
520 primary production using observations and models. *Global Biogeochemical Cycles*,
521 *27*(3), 847–858. https://doi.org/10.1002/gbc.20074
522 Clement, D., & Gruber, N. (2018). The eMLR(C*) Method to Determine Decadal Changes in the
523 Global Ocean Storage of Anthropogenic CO2. *Global Biogeochemical Cycles*, *32*(4),
524 654–679. https://doi.org/10.1002/2017GB005819
525 DeVries, T., Holzer, M., & Primeau, F. (2017). Recent increase in oceanic carbon uptake driven
526 by weaker upper-ocean overturning. *Nature*, *542*(7640), 215–218.
527 https://doi.org/10.1038/nature21068
528 DeVries, T., Le Quéré, C., Andrews, O., Berthet, S., Hauck, J., Ilyina, T., et al. (2019). Decadal
529 trends in the ocean carbon sink. *Proceedings of the National Academy of Sciences*,
530 201900371. https://doi.org/10.1073/pnas.1900371116
531 Downes, S. M., Langlais, C., Brook, J. P., & Spence, P. (2017). Regional Impacts of the
532 Westerly Winds on Southern Ocean Mode and Intermediate Water Subduction. *Journal*
533 *of Physical Oceanography*, *47*(10), 2521–2530. https://doi.org/10.1175/JPO-D-17-0106.1
534 Fox-Kemper, B., Hewitt, H. T., Xiao, C., Aðalgeirsdóttir, G., Drijfhout, S. S., Edwards, T. L., et

al. (2021). Ocean, Cryosphere and Sea Level Change. *Climate Change 2021: The Physical 12 Science Basis. Contribution of Working Group I to the Sixth Assessment Report of the Intergovernmental 13 Panel on Climate Change*.

Friedlingstein, P., Jones, M. W., O'Sullivan, M., Andrew, R. M., Bakker, D. C. E., Hauck, J., et al. (2021). Global Carbon Budget 2021. *Earth System Science Data Discussions*, 1–191. https://doi.org/10.5194/essd-2021-386

Fyfe, J. C., & Saenko, O. A. (2006). Simulated changes in the extratropical Southern Hemisphere winds and currents. *Geophysical Research Letters*, *33*(6). https://doi.org/10.1029/2005GL025332

Gloege, L., McKinley, G. A., Landschützer, P., Fay, A. R., Frölicher, T. L., Fyfe, J. C., et al. (2021). Quantifying Errors in Observationally Based Estimates of Ocean Carbon Sink Variability. *Global Biogeochemical Cycles*, *35*(4), e2020GB006788. https://doi.org/10.1029/2020GB006788

Gruber, N., Clement, D., Carter, B. R., Feely, R. A., van Heuven, S., Hoppema, M., et al. (2019a). The oceanic sink for anthropogenic CO_2 from 1994 to 2007. *Science*, *363*(6432), 1193–1199. https://doi.org/10.1126/science.aau5153

Gruber, N., Landschützer, P., & Lovenduski, N. S. (2019b). The Variable Southern Ocean Carbon Sink. *Annual Review of Marine Science*, *11*(1), 159–186. https://doi.org/10.1146/annurev-marine-121916-063407

Hauck, J., Zeising, M., Le Quéré, C., Gruber, N., Bakker, D. C. E., Bopp, L., et al. (2020). Consistency and Challenges in the Ocean Carbon Sink Estimate for the Global Carbon Budget. *Frontiers in Marine Science*, *7*. https://doi.org/10.3389/fmars.2020.571720

Keppler, L., & Landschützer, P. (2019). Regional Wind Variability Modulates the Southern

Ocean Carbon Sink. *Scientific Reports*, *9*(1), 7384. https://doi.org/10.1038/s41598-019-43826-y

Landschützer, P., Gruber, N., Haumann, F. A., Rödenbeck, C., Bakker, D. C. E., Van Heuven, S., et al. (2015). The reinvigoration of the Southern Ocean carbon sink. *Science*, *349*(6253), 1221–1224. https://10.1126/science.aab2620

Le Quéré, C., Rödenbeck, C., Buitenhuis, E. T., Conway, T. J., Langenfelds, R., Gomez, A., et al. (2007). Saturation of the Southern Ocean CO_2 Sink Due to Recent Climate Change. *Science*, *316*(5832), 1735–1738. https://doi.org/10.1126/science.1136188

Le Quéré, C., Buitenhuis, E. T., Moriarty, R., Alvain, S., Aumont, O., Bopp, L., et al. (2016). Role of zooplankton dynamics for Southern Ocean phytoplankton biomass and global biogeochemical cycles. *Biogeosciences Discussions*, *12*(14), 11935–11985. https://doi.org/10.5194/bgd-12-11935-2015

Lenton, A., Tilbrook, B., Law, R. M., Bakker, D., Doney, S. C., Gruber, N., et al. (2013). Sea–air CO_2 fluxes in the Southern Ocean for the period 1990-2009. *Biogeosciences*, *10*(6), 4037–4054. https://doi.org/10.5194/bg-10-4037-2013

MacGilchrist, G. A., Naveira Garabato, A. C., Brown, P. J., Jullion, L., Bacon, S., Bakker, D. C. E., et al. (2019). Reframing the carbon cycle of the subpolar Southern Ocean. *Science Advances*, *5*(8), 1–9. https://doi.org/10.1126/sciadv.aav6410

Madec, G. (2013). NEMO ocean engine. *Note Du Pole de Modélisation de Institut Pierre-Simon Laplace (IPSL)*, *27*. https://doi.org/10.5281/zenodo.1464817

McKinley, G. A., Fay, A. R., Eddebbar, Y. A., Gloege, L., & Lovenduski, N. S. (2020). External Forcing Explains Recent Decadal Variability of the Ocean Carbon Sink. *AGU Advances*, *1*(2), e2019AV000149. https://doi.org/10.1029/2019AV000149

581 Meredith, M., Sommerkorn, M., Cassotta, S., Derksen, C., Ekaykin, A., Hollowed, A., et al.
582 (2019). Polar Regions. In H. O. Pörtner, D. C. Roberts, V. Masson-Delmotte, P. Zhai, M.
583 Tignor, E. Poloczanska, et al. (Eds.), *IPCC Special Report on the Ocean and Crysphere*
584 *in a Changing Climate*.
585 Morrison, A. K., Waugh, D. W., Hogg, A. M., Jones, D. C., & Abernathey, R. P. (2021).
586 Ventilation of the Southern Ocean Pycnocline, 26. https://doi.org/10.1146/annurev-
587 marine-010419-011012
588 Olsen, A., Lange, N., Key, R. M., Tanhua, T., Bittig, H. C., Kozyr, A., et al. (2020).
589 *GLODAPv2.2020 – the second update of GLODAPv2* (preprint). Oceanography –
590 Chemical. https://doi.org/10.5194/essd-2020-165
591 Patara, L., Böning, C. W., & Tanhua, T. (2021). Multidecadal Changes in Southern Ocean
592 Ventilation since the 1960s Driven by Wind and Buoyancy Forcing. *Journal of Climate*,
593 *34*(4), 1485–1502. https://doi.org/10.1175/JCLI-D-19-0947.1
594 Sallée, J. B., Speer, K. G., & Rintoul, S. R. (2010). Zonally asymmetric response of the Southern
595 Ocean mixed-layer depth to the Southern Annular Mode. *Nature Geoscience*, *3*(4), 273–
596 279. https://doi.org/10.1038/ngeo812
597 Thompson, D. W. J., & Solomon, S. (2002). Interpretation of Recent Southern Hemisphere
598 Climate Change. *Science*, *296*(5569), 895–899. https://doi.org/10.1126/science.1069270
599 Thompson, D. W. J., Solomon, S., Kushner, P. J., England, M. H., Grise, K. M., & Karoly, D. J.
600 (2011). Signatures of the Antarctic ozone hole in Southern Hemisphere surface climate
601 change. *Nature Geoscience*, *4*(11), 741–749. https://doi.org/10.1038/ngeo1296
602 Timmermann, R., Goosse, H., Madec, G., Fichefet, T., Ethe, C., & Duliere, V. (2005). On the
603 representation of high latitude processes in the ORCA-LIM global coupled sea ice–ocean

model. *Ocean Modelling*, *8*(1–2), 175–201.
https://doi.org/10.1016/j.ocemod.2003.12.009

Wright, R. M., Le Quéré, C., Buitenhuis, E., Pitois, S., & Gibbons, M. J. (2021). Role of jellyfish in the plankton ecosystem revealed using a global ocean biogeochemical model. *Biogeosciences*, *18*(4), 1291–1320. https://doi.org/10.5194/bg-18-1291-2021